A new numerical path to retrieve isolated branches on large scale nolinear mechanical systems

Samuel Quaegebeur, Thibaut Vadcard, Fabrice Thouverez

A new numerical path to retrieve isolated branches on large scale nolinear mechanical systems

Samuel Quaegebeur[1], Thibaut Vadcard[1], and Fabrice Thouverez[1]

Abstract

In the domain of vibrations, the response of a mechanical system is often depicted as the amplitude versus the excitation frequency, namely the frequency response. For a given value of the excitation frequency, the uniqueness of the solution to the structural dynamics problem is not ensured in a nonlinear framework. Given this property, continuation techniques should be employed as a way of computing the entire response of a structure, also called the Nonlinear Frequency Response Curve (NFRC). It was shown in the literature that some branches of solutions–named isolas–can even be isolated from the primary response curve of the system. The systematic computation of theses branches of solutions is challenging and remains an active field of research. In this work, a novel approach is proposed to seek solutions in another search space to obtain the force amplitude response (FAR) of the system. Providing relevant information when the excitation frequency is known, the solutions can also be used as initialization points to evaluate traditional NFRC. The methodology will be shown to be highly versatile and relevant to compute nonlinear solutions. It will be employed for different mechanical systems and nonlinearities with an increasing level of complexity. The strategy allows to detect numerous types of isolas (primary, subharmonic, superharmonic, and ultra-subharmonic resonances), even for an industrial fan blade.

Keywords

Harmonic Balance Method, Isola, Geometric nonlinearities, Bifurcation theory, Large scale systems

1 - École Centrale de Lyon, Laboratoire de Tribologie et Dynamique des Systèmes, UMR CNRS 5513, 36 avenue Guy de Collongue, Écully, 69134, France

1 Introduction

Mechanical systems are seldom linear: the material of the structures, its large displacements, its interaction with others systems (fluid or solid), are sources of nonlinearities which give rise to complex dynamics behaviours. In a world where optimization is becoming of the utmost importance, especially for environmental considerations, designing systems while including its inherent nonlinearities is necessary.

Nonlinear systems feature many different behaviours and types of solutions [1]. In this work, the emphasis is on periodic solutions that are detached from the primary frequency response curve, termed isolas [2]. These types of solutions have been the subject of many studies in the past decade. They have been observed in experiments through modal interaction [3], with continuation based control [4] but also through phase-locked-loop techniques [5, 6]. These papers show that isolas exist in real systems, hence it has become important to predict their occurrence numerically.

Different methodologies, including analytical tools, have been proposed to compute these isolas. The multiple scales approach has been used in several studies to demonstrate their existence: for impact systems [7] and for two coupled Duffing oscillators [8]. Using singular theory and averaging method, Habib et al. [9] unveiled relationships between nonlinear damping and isolated branches. The theory of spectral submanifolds was also successfully employed to retrieve these detached solutions [10].

Isolas have been widely uncovered through numerical simulations. Many of them use the Harmonic Balance Method [11] to recast the equations of motion into an algebraic set of equations. With this new system, different methods have been proposed to retrieve isolas. For low dimensional systems and polynomial nonlinearities, the Groebner basis was employed to evaluate all the solutions of the problem [12]. Heinze et al. [13] proposed a global terrain approach. This strategy was applied to large scale systems with friction nonlinearities.

Recently, researchers brought to light a relationship between nonlinear normal modes and isolas [14]. Cenedese and Haller [15] presented a Melnikov function analysis to detect multiple solutions in the vicinity of a nonlinear normal mode. This strategy was the successfully employed for the research of isolated solutions for systems featuring dry friction on a parametric oscillator [16], impact nonlinearities [17] and blade-tip/casing contacts [18].

From the HBM system of equations, the nonlinear frequency response curve (NFRC) of a mechanical system can be evaluated with continuation algorithm [19]. Moreover, the bifurcation theory [20] has been employed together with the HBM to retrieve bifurcated branches and isolas [21, 22]. It has also been used with an homotopy procedure to evaluate different solutions including isolas [13, 23]. Different papers have used the bifurcation theory to locate and track bifurcations points [24, 25], which may connect primary frequency response curves with isolated solutions in an augmented space. An extension of such algorithms has been provided for period-doubling bifurcations [26]. Locating the extremums points and tracking them in different dimensions was shown to detect isolas [27, 28]. Using the HBM and bifurcation tracking, [29] proposes a framework to control the location of isolas.

This paper proposes a new methodology based on the HBM and bifurcation theory to retrieve isolas. Its originality lies in the search space of the solutions. They are evaluated along the excitation amplitude as a continuation parameter instead of the excitation frequency. These new curves termed Force Amplitude Responses (FAR) may find analogy in the so-called S-curve obtained in the continuation based control experiment [4]. However, in this paper, a numerical methodology is proposed to retrieve these branches of solutions for any kind of resonances. This new vision of the response of the system provide relevant information for the characterization of nonlinear systems. First, in many situations, the excitation frequency is known, set by external conditions, however its amplitude is subjected to changes and can only be estimated. The FAR curve then takes all its meaning and the different solutions of the problem can be immediately obtained. Conversely, the FAR results provide initialization points for standard NFRC (when the excitation amplitude is known but not its frequency).

The numerical tools used in this paper are described in Section 2. The derivations of the new methodology are then provided in Section 3. This approach is used for academic test cases with different nonlinearities in Section 4. Finally, an industrial test case, featuring blade-tip/casing contacts, is considered in Section 5.

2 Numerical tools to evaluate the frequency response

This section aims to present the required numerical techniques to compute NFRF as well as to provide an illustrative example.

2.1 Numerical implementation

As periodic solutions are sought, the HBM is employed and is explained next. The other sections are devoted to explain how the HBM can be used with the bifurcation theory to obtain bifurcated branches.

2.1.1 Harmonic Balance Method

The motion equations of a nonlinear mechanical system are

$$\mathbf{M}\ddot{\mathbf{x}}\left(t\right)+\mathbf{C}\dot{\mathbf{x}}\left(t\right)+\mathbf{K}\mathbf{x}\left(t\right)+\mathbf{f}_{\mathrm{nl}}\left(\mathbf{x},\dot{\mathbf{x}}\right)-\mathbf{f}_{\mathrm{ext}}\left(t\right)=\mathbf{0}. \tag{1}$$

The matrices $\mathbf{M}$, $\mathbf{C}$, and $\mathbf{K}$ are respectively the mass, damping and stiffness matrices. Vectors $\mathbf{x}$, $\mathbf{f}_{\mathrm{nl}}$, and $\mathbf{f}_{\mathrm{ext}}$ denote the displacement of the system, the nonlinear and external forces. The excitation is $\frac{2\pi}{\omega}$ periodic, ω being the excitation frequency. In this work, the emphasis is on the research of periodic solutions, thus the displacement is chosen to be sought as a periodic response in the form of a Fourier series of order N_h. Moreover, to account for possible subharmonic and ultra-subharmonic resonances, the response uses the positive integer ν,

$$\mathbf{x}_{\nu}\left(t\right)=\frac{\mathbf{a}_0}{2}+\sum_{k=1}^{N_h}\left(\mathbf{a}_{\nu,k}\cos\left(\frac{k}{\nu}\omega t\right)+\mathbf{b}_{\nu,k}\sin\left(\frac{k}{\nu}\omega t\right)\right). \tag{2}$$

The coefficients $\mathbf{a}_0$, $\left(\mathbf{a}_{\nu,k},\,\mathbf{b}_{\nu,k}\right)_{k\in[\![1,N_h]\!]}$ denote the real Fourier coefficients. Substituting Equation Eq. (2) in Eq. (1), and projecting on the trigonometric basis with the scalar product

$$\left\langle f,g\right\rangle=\frac{\omega}{\pi}\int_0^{\frac{2\pi}{\omega}}f\left(t\right)g\left(t\right)\mathrm{d}t \tag{3}$$

gives

$$\begin{cases}\mathbf{Z}_0\mathbf{a}_0+\left(\mathbf{c}_{f_{\mathrm{nl},0}}-\mathbf{c}_{f_{\mathrm{ext},0}}\right)=\mathbf{0} & \text{(4a)}\\ \mathbf{Z}_{\nu,k}\begin{bmatrix}\mathbf{a}_{\nu,k}\\ \mathbf{b}_{\nu,k}\end{bmatrix}+\begin{bmatrix}\left(\mathbf{c}_{f_{\mathrm{nl},c,\nu,k}}-\mathbf{c}_{f_{\mathrm{ext},c,\nu,k}}\right)\\ \left(\mathbf{c}_{f_{\mathrm{nl},s,\nu,k}}-\mathbf{c}_{f_{\mathrm{ext},s,\nu,k}}\right)\end{bmatrix}=\begin{bmatrix}\mathbf{0}\\ \mathbf{0}\end{bmatrix},\forall k\in[\![1,N_h]\!]. & \text{(4b)}\end{cases}$$

The matrix $\mathbf{Z}_{\nu,k}$ is the dynamic matrix and is equal to

$$\begin{cases}\mathbf{Z}_0=\mathbf{K} & \text{(5a)}\\ \mathbf{Z}_{\nu,k}=\omega^2\left(\nabla_{\nu,k}\otimes\mathbf{M}\right)+\omega\left(\nabla_{\nu,k}\otimes\mathbf{C}\right)+\left(\mathbf{I}_2\otimes\mathbf{K}\right), & \text{(5b)}\end{cases}$$

where $\mathbf{I}_2$ is the identity matrix of size 2, and

$$\nabla_{\nu,k}=\begin{bmatrix}0 & \frac{k}{\nu}\\ -\frac{k}{\nu} & 0\end{bmatrix}. \tag{6}$$

In the following, the term ∇_{f} denotes the block diagonal matrix constituted of all $\left(\nabla_{\nu,k}\right)_{k\in[\![0,N_h]\!]}$, with $\nabla_{\nu,0}=0$. The terms $\mathbf{c}_{f_{\mathrm{ext},1}}$, $\mathbf{c}_{f_{\mathrm{ext},c,\nu,k}}$, and $\mathbf{c}_{f_{\mathrm{ext},s,\nu,k}}$ correspond to the projection of the external forces on the functions 1, $\cos\left(\frac{k}{\nu}\omega t\right)$, and $\sin\left(\frac{k}{\nu}\omega t\right)$, respectively. A similar operation is applied to the nonlinear forces, denoted by $\mathbf{c}_{f_{\mathrm{nl}}}$. However these forces do not have an analytic formulation in the frequency domain and are thus evaluated through an Alternating Frequency Time procedure [30]: the displacement is evaluated for a discretized time period through Equation Eq. (2)

(with a matrix Γ) to compute the nonlinear forces in the time domain. Those are then transformed to the frequency domain with the matrix Γ^{-1}. Gathering the different terms in Equation Eq. (4) gives the residual

$$\mathbf{r}(\mathbf{c}) = \mathbf{Z}\mathbf{c} + \mathbf{c}_{f_{\text{nl}}} - \mathbf{c}_{f_{\text{ext}}} = \mathbf{0}, \tag{7}$$

where $\mathbf{Z}$ denotes the dynamic stiffness matrix of all harmonics k, and $\mathbf{c}$ gathers the different Fourier coefficients $\left[\mathbf{a}_0^\intercal, \cdots, \mathbf{a}_{\nu,k}^\intercal, \mathbf{b}_{\nu,k}^\intercal\right]^\intercal$. The vectors $\mathbf{c}_{f_{\text{nl}}}$ and $\mathbf{c}_{f_{\text{ext}}}$ correspond to the projection of the nonlinear and external forces on the full basis. To solve the nonlinear system of equations Eq. (7), a Newton-Raphson solver is used. To ensure fast computation, the jacobian of the system is analytically computed. The jacobian matrix of the residual function Eq. (7), with respect to the unknowns $\mathbf{c}$, is noted $\mathbf{J}_\mathbf{c}$. In the following, the derivative of the residual with respect to ω is noted $\mathbf{J}_\omega$.

To account for multiple solutions of a nonlinear response, an arc-length procedure [19] is employed. The scalar ω becomes an additional unknown of the problem, thus a supplementary equation should be included in the set of equations to have a square system

$$(\mathbf{c} - \mathbf{c}_p)^\intercal (\mathbf{c} - \mathbf{c}_p) + (\omega - \omega_p)^2 - \mathrm{d}s^2 = 0, \tag{8}$$

where the couple $(\omega_p, \mathbf{c}_p)$ is a previously obtained solution of the system and $\mathrm{d}s$ is the arc-length step. The solution curve is thus parameterized by the curvilinear abscissa s.

2.1.2 Determination of the bifurcated points

Nonlinear systems have the particularity of admitting several solutions for the same excitation frequency. Some of these solutions are connected to the primary branch of solution through bifurcation points. Different strategies exist to evaluate such points: through the Hill method [25], or also by test functions [24]. The former approach is employed here as it also enables to retrieve the stability of the solution. Hill's method requires to solve the following quadratic eigenvalue problem

$$\left(\mathbf{J}_\mathbf{c} + \Delta_1\lambda + \Delta_2\lambda^2\right)\phi = \mathbf{0}, \tag{9}$$

where Λ and ϕ are the eigenvalues and eigenvectors of the problem. Furthermore, the others terms are defined as

$$\begin{cases} \Delta_1 = 2\omega_\text{s}\left(\nabla_\mathbf{f} \otimes \mathbf{M}\right) + \mathbf{I}_{2N_h+1} \otimes \mathbf{C} + \Gamma^{-1}\dfrac{\partial \mathbf{f}_\text{nl}}{\partial \dot{\mathbf{x}}}\Gamma & \text{(10a)} \\ \Delta_2 = \mathbf{I}_{2N_h+1} \otimes \mathbf{M}. & \text{(10b)} \end{cases}$$

Notice that the term $\Gamma^{-1}\frac{\partial \mathbf{f}_\text{nl}}{\partial \dot{\mathbf{x}}}\Gamma$ is oftentimes forgotten in the literature [25] but is highlighted by some authors [31, 32]. The eigenvalues (which correspond to the Floquet exponents) are used to determine the nature of the bifurcations point that is encountered. Bifurcation points are obtained when λ crosses the imaginary axis. If $\lambda = 0$, a limit or branching point is detected. If $\lambda = \pm\mathrm{i}\frac{\omega}{2}$ (where i is the complex number), it is a period doubling bifurcation point. Otherwise, it corresponds to a Neimark-Sacker bifurcation point. This latter case describes branches of quasi-periodic solution which are beyond the scope of this paper. Periodic bifurcated branches will be the focus of this paper.

When a branching point is detected, one must find its exact location before computing the tangent of the different branches of solutions emerging from this point [20, 33]. These tangents are computed so that each new branch can be followed through a path following procedure. The computation of the exact location of the branching point requires to solve the following system

$$\begin{cases} \mathbf{r}(\mathbf{c}, \omega) + \gamma\mathbf{h} = \mathbf{0}, & \text{(11a)} \\ \mathbf{J}_\mathbf{c}^\intercal\mathbf{h} = \mathbf{0}, & \text{(11b)} \\ \mathbf{J}_\omega^\intercal\mathbf{h} = 0, & \text{(11c)} \\ \mathbf{h}^\intercal\mathbf{h} - 1 = 0 & \text{(11d)} \end{cases}$$

where $(\mathbf{c}, \omega, \mathbf{h}, \gamma)$ are the unknowns of the problems. This problem is solved using a Newton-Raphson procedure. To ensure fast computation, the jacobian of this problem should be provided, and hence the analytical evaluation of the hessian tensor of the nonlinear forces is required. The solution of this problem is noted $(\mathbf{c}_\mathrm{s}, \omega_\mathrm{s}, \mathbf{h}_\mathrm{s}, \gamma_\mathrm{s})$. The system of equations Eq. (11) is specific for locating branching points. If one is interested in other bifurcations points, different system of equations must be solved [25, 26].

2.1.3 Determination of the tangent of the bifurcation points

The tangents of the branches of solutions are then derived, noted by $\mathbf{t} = \left[\left(\frac{\partial \mathbf{c}}{\partial s}_{|_{\mathbf{c}_\mathrm{s}}}\right)^\intercal, \frac{\partial \omega}{\partial s}_{|_{\omega_\mathrm{s}}}\right]^\intercal$. The tangents are a linear combination of the vectors $\mathbf{v}_1$ and $\mathbf{v}_2$ which constitute a basis of the kernel of $[\mathbf{J}_\mathbf{c}, \mathbf{J}_\omega]$,

$$\mathbf{t} = \alpha_1 \mathbf{v}_1 + \alpha_2 \mathbf{v}_2. \tag{12}$$

To evaluate the tangent, one must determine the couple (α_1, α_2). To this end, the residual (see Equation Eq. (7)) is differentiated twice with respect to the curvilinear abscissa s and evaluated at the bifurcation point,

$$\begin{aligned}
\frac{\partial^2}{\partial s^2}\left(\mathbf{r}\left(\mathbf{c}, \omega\right)\right)_{|_{(\mathbf{c}_\mathrm{s}, \omega_s)}} &= \mathbf{0}, \\
\frac{\partial}{\partial s}\left(\frac{\partial \mathbf{r}}{\partial \mathbf{c}}\frac{\partial \mathbf{c}}{\partial s} + \frac{\partial \mathbf{r}}{\partial \omega}\frac{\partial \omega}{\partial s}\right)_{|_{(\mathbf{c}_\mathrm{s}, \omega_s)}} &= \mathbf{0}, \\
\left(\frac{\partial \mathbf{r}}{\partial \mathbf{c}}\frac{\partial^2 \mathbf{c}}{\partial s^2} + \frac{\partial \mathbf{r}}{\partial \omega}\frac{\partial^2 \omega}{\partial s^2}\right)_{|_{(\mathbf{c}_\mathrm{s}, \omega_s)}} + \left(\frac{\partial^2 \mathbf{r}}{\partial \mathbf{c}^2}\frac{\partial \mathbf{c}}{\partial s}\frac{\partial \mathbf{c}}{\partial s} + 2\frac{\partial^2 \mathbf{r}}{\partial \omega \partial \mathbf{c}}\frac{\partial \mathbf{c}}{\partial s}\frac{\partial \omega}{\partial s} + \frac{\partial^2 \mathbf{r}}{\partial^2 \omega}\left(\frac{\partial \omega}{\partial s}\right)^2\right)_{|_{(\mathbf{c}_\mathrm{s}, \omega_s)}} &= \mathbf{0}.
\end{aligned} \tag{13}$$

The first term is cumbersome to compute since the derivative of the tangent with respect to the curvilinear abscissa is unknown. To remove this term, the equation is multiplied by the basis of the kernel of $[\mathbf{J}_\mathbf{c}^\intercal, \mathbf{J}_\omega]^\intercal$. The dimension of such space is equal to 1 and the basis is noted $\mathbf{g}$. This operation gives

$$\mathbf{g}^\intercal\left(\frac{\partial^2 \mathbf{r}}{\partial \mathbf{c}^2}\frac{\partial \mathbf{c}}{\partial s}\frac{\partial \mathbf{c}}{\partial s} + 2\frac{\partial^2 \mathbf{r}}{\partial \omega \partial \mathbf{c}}\frac{\partial \mathbf{c}}{\partial s}\frac{\partial \omega}{\partial s} + \frac{\partial^2 \mathbf{r}}{\partial^2 \omega}\left(\frac{\partial \omega}{\partial s}\right)^2\right)_{|_{(\mathbf{c}_\mathrm{s}, \omega_s)}} = 0. \tag{14}$$

This equation is written in a more compact form

$$\mathbf{g}^\intercal\left(\mathbf{H}_{|_{(\mathbf{c}_\mathrm{s}, \omega_s)}}\left(\mathbf{t}, \mathbf{t}\right)\right) = 0, \tag{15}$$

where $\mathbf{H}_{|_{(\mathbf{c}_\mathrm{s}, \omega_s)}}\left(\mathbf{t}, \mathbf{t}\right)$ is the hessian of the residual at the bifurcation point multiplied twice by the tangent vector. Substituting Eq. (12) in Equation Eq. (15) gives the following quadratic form

$$b_{11}\alpha_1^2 + 2b_{12}\alpha_1\alpha_2 + b_{22}\alpha_2^2 = 0, \tag{16}$$

where $b_{ij} = \mathbf{g}^\intercal\left(\mathbf{H}_{|_{(\mathbf{c}_\mathrm{s}, \omega_s)}}\left(\mathbf{t}_i, \mathbf{t}_j\right)\right)$. In matrix form, this is written

$$\alpha^\intercal \mathbf{B} \alpha = 0, \tag{17}$$

where α and $\mathbf{B}$ contain the values α_i and b_{ij} respectively. The matrix $\mathbf{B}$, being symmetric, may be written as $\mathbf{P}\mathbf{D}\mathbf{P}^\intercal$, where $\mathbf{P}$ is an orthogonal matrix (with components p_{ij}) and $\mathbf{D}$ is a diagonal matrix (with components d_i). Defining $\beta = \mathbf{P}^\intercal \alpha$, Equation Eq. (17) is equivalent to

$$\beta_1^2 d_1 + \beta_2^2 d_2 = 0. \tag{18}$$

This equation is much simpler to solve than Eq. (16) but still contains two unknowns. To obtain a square system, the norm of the tangent vector is imposed to be equal to $\mathrm{d}s$,

$$\begin{aligned}
\|\mathbf{t}\| &= \mathrm{d}s \\
\|\left(p_{11}\beta_1 + p_{12}\beta_2\right)\mathbf{t}_1 + \left(p_{21}\beta_1 + p_{22}\beta_2\right)\mathbf{t}_2\| &= \mathrm{d}s
\end{aligned} \tag{19}$$

Solving Equations Eq. (18) and Eq. (19) allows determining β, hence α, and finally the tangents $\mathbf{t}$. The bifurcated branch can then be computed by solving Equation Eq. (7) and Eq. (8) with an initialization point chosen along the tangent.

2.2 Illustrative numerical example

In the rest of this section, a simple test case is considered to illustrate the numerical tools explained above. This same example will be used with the new methodology in Section 3.2.

2.2.1 Description of the test case

A cyclic symmetric system constituted of Duffing oscillators is studied. It is depicted in Figure 1. A similar test case was proposed in [12]. The parameters are provided in Table 1. A cubic nonlinearity, $f_{\text{nl}} = k_{\text{nl}} x\,(t)^3$ is applied to each degree of freedom (DOF) of the system. An uniform excitation is applied to the mechanical system,

$$\mathbf{f}_{\text{ext}} = [1, 1, 1, 1]^{\intercal}\,. \tag{20}$$

The HBM is employed with $N_h = 15$ harmonics and the period is discretized through 200 instants for the AFT procedure.

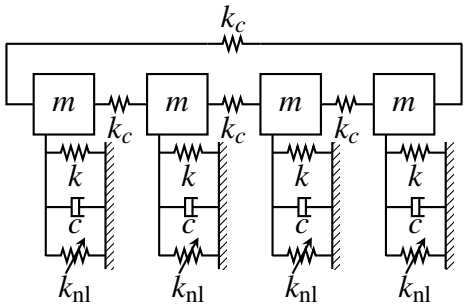

Figure 1. Cyclic symmetric system.

Parameters	m	k	c	k_c	k_{nl}
Values	1	1	0.1	1	1

Table 1. Structural parameters of the cyclic symmetric example.

2.3 Numerical results

Examples of NFRC functions of such a system is provided in Figure 2 for two excitation levels, i.e. 1 N and 2 N. For both cases, superharmonic responses are observed at low frequencies (below 1 rad·s^{-1}). For the 1 N excitation level (see Figure 2a), the 1 : 1 resonance peak is located at 3 rad·s^{-1} and for this level of forcing, no bifurcations points are detected.

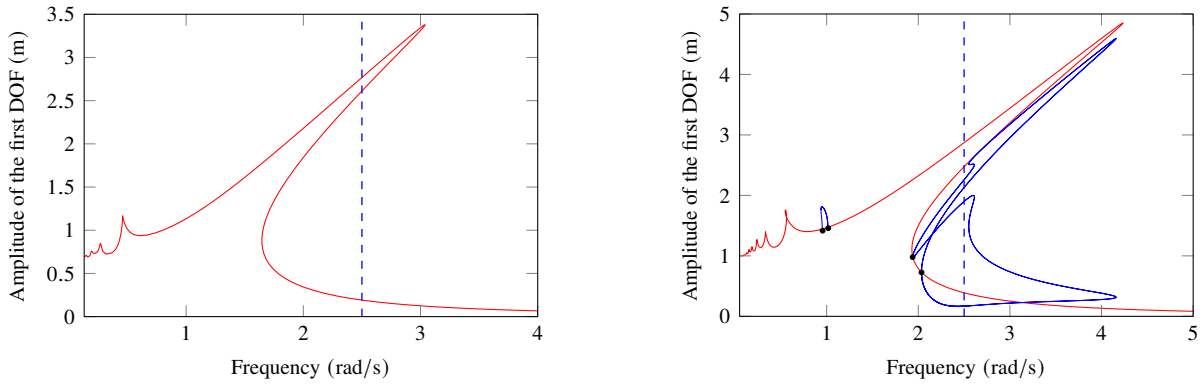

(a) 1 N excitation level. **(b)** 2 N excitation level.

Figure 2. NFRC for different excitation levels. Primary curve (—), bifurcated branches (—), and branching points (●). The dashed blue line (- -) corresponds to the search space $\omega = 2.5\,\mathrm{rad{\cdot}s^{-1}}$ of the future methodology.

In Figure 2b, the level of forcing is increased up to 2 N. Bifurcations points are detected and the associated branches of solutions followed. Around $1\,\mathrm{rad{\cdot}s^{-1}}$, the bifurcation corresponds to a $2:1$ superharmonic response whereas the curve at higher excitation frequencies correspond to a $1:1$ resonance.

The tools employed, however, do not permit to retrieve eventual isolated branches. The key idea of this paper is to search solution at a fixed frequency for all forcing/displacement amplitudes, as depicted through the blue lines (- -) in Figures 2a and 2b, located at $\omega = 2.5\,\mathrm{rad{\cdot}s^{-1}}$. The methodology used to compute the curve that links all solutions for variable forcing amplitudes is presented in Section 3.

3 New formulation: force amplitude response

In this section, the evaluation of FAR is proposed. As it will be explained below, such curve allows providing new initialization points of the strategy proposed in Section 2.1.1 to compute isolated frequency responses.

3.1 Description of the methodology

The problem defined in Equation Eq. (1) is considered with the following modifications. First, the excitation forces are sought as

$$\mathbf{f}_{\mathrm{ext}}\left(t\right) = f_a \mathbf{f}_{\mathrm{ext},s}\left(t\right), \tag{21}$$

where $\mathbf{f}_{\mathrm{ext},s}$ is the shape of the external forces and the scalar f_a is the excitation amplitude, here unknown. Second, the harmonics $\mathbf{c}$, defined in Equation Eq. (7) are split into an imposed part (subscripted i), and an unknown part (subscripted r). Here, the harmonic $a_{\nu,k}$ of an arbitrary DOF is imposed. Equation Eq. (7) is thus split into

$$\begin{bmatrix} Z_{\mathrm{ii}} & \mathbf{Z}_{\mathrm{ir}} \\ \mathbf{Z}_{\mathrm{ri}} & \mathbf{Z}_{\mathrm{rr}} \end{bmatrix} \begin{bmatrix} a_{\nu,k} \\ \mathbf{c}_{\mathrm{r}} \end{bmatrix} + \begin{bmatrix} c_{f_{\mathrm{nl}},\mathrm{i}} \\ \mathbf{c}_{f_{\mathrm{nl}},\mathrm{r}} \end{bmatrix} = \begin{bmatrix} c_{f_{\mathrm{ext}},\mathrm{i}} \\ \mathbf{c}_{f_{\mathrm{ext}},\mathrm{r}} \end{bmatrix} f_a \tag{22}$$

The unknowns are gathered and the system is thus re-arranged into

$$\begin{bmatrix} c_{f_{\mathrm{ext}},\mathrm{i}} & \mathbf{Z}_{\mathrm{ir}} \\ \mathbf{c}_{f_{\mathrm{ext}},\mathrm{r}} & \mathbf{Z}_{\mathrm{rr}} \end{bmatrix} \begin{bmatrix} f_a \\ \mathbf{c}_{\mathrm{r}} \end{bmatrix} + \begin{bmatrix} c_{f_{\mathrm{nl}},\mathrm{i}} \\ \mathbf{c}_{f_{\mathrm{nl}},\mathrm{r}} \end{bmatrix} = \begin{bmatrix} Z_{\mathrm{ii}} \\ \mathbf{Z}_{\mathrm{ri}} \end{bmatrix} a_{\nu,k} \tag{23}$$

For the first iteration of the methodology, Equation Eq. (23) is solved with $a_{\nu,k}$ set at a value x_0. Then a continuation procedure is employed with the additional arc length equation to account for possible limit points and multiple solutions,

$$\left(f_a - f_{a,p}\right)^2 + \left(\mathbf{c}_{\mathrm{r}} - \mathbf{c}_{\mathrm{r},p}\right)^{\intercal}\left(\mathbf{c}_{\mathrm{r}} - \mathbf{c}_{\mathrm{r},p}\right) + \left(a_{\nu,k} - a_{\nu,k,p}\right)^2 - \mathrm{d}s^2 = 0, \tag{24}$$

where $(f_{a,p}, \mathbf{c}_{r,p}), a_{\nu,k,p}$ is the previous solution of the system (iteration p). Solving this set of equations enables to obtain a curve of solutions at a fixed excitation frequency ω. The numerical tools presented in Sections 2.1.2 and 2.1.3, i.e. determination of the bifurcated points and their associated tangents, are also employed with this strategy, with the slight change of switching the unknown ω with f_a.

3.2 Application of the proposed strategy

The methodology is now applied to the mechanical system illustrated in Figure 1 for a frequency set at $\omega = 2.5\,\mathrm{rad{\cdot}s^{-1}}$. The shape of the excitation is equal to Equation Eq. (20). The evolution of the force level with respect of the first DOF amplitude is illustrated in Figure 3a. The red curve corresponds to the main resonance response whereas green curves are the bifurcated solutions. For better readability, only the bifurcated branches arising from the main response are presented in Figure 3a. Computing bifurcated branches of the already bifurcated branches leads to the discovery of Figure 3b

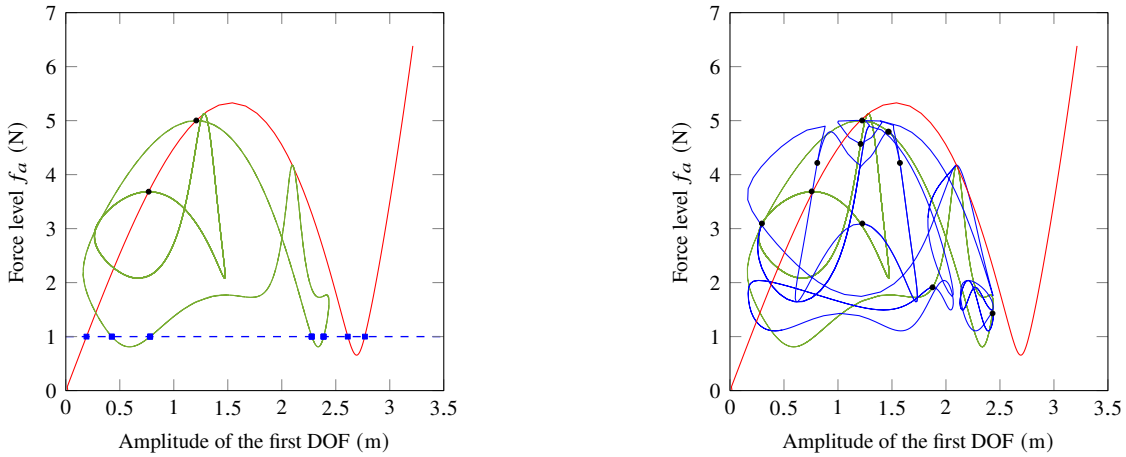

(a) Bifurcated branches from the primary curve.

(b) All bifurcated branches

Figure 3. FAR with $\omega = 2.5\,\mathrm{rad{\cdot}s^{-1}}$, primary curve (—), bifurcated branches (—), additional bifurcated branches (—), branching points (●). $f_a = 1\,\mathrm{N}$ (- -), solutions at $f_a = 1\,\mathrm{N}$ (■).

The result of Figure 3a gives initialization points that can be used to obtain the full NFRC of the mechanical system. First, one must chose an excitation amplitude and find the intersecting solutions points. Such procedure is depicted in Figure 3a through the blue line located at 1 N and the blue square markers. Then, the NFRC can then be obtained classically (with the resolution of Equations Eq. (7) and Eq. (8)) with an initialization on the aforementioned solutions points. The responses of this strategy are depicted in Figure 4. Compared to the traditional approach, two new isolated curves are obtained.

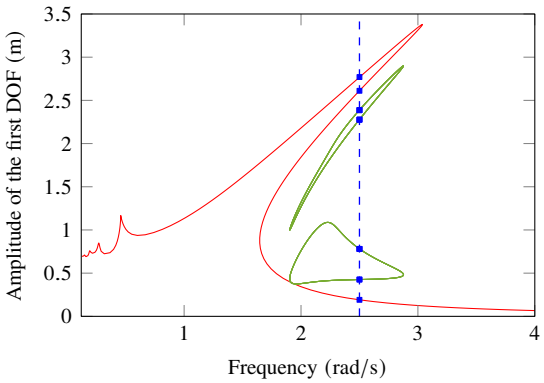

Figure 4. NFRC with 1 N excitation level, primary curve (—), isolated branches (—), $f_a = 1\,\mathrm{N}$ (—), solutions found along the FAR of Figure 3a (■).

Figures 5 and 6 provide NFRC for different level of excitation amplitudes, obtained with the proposed strategy. For the primary solution branch (Figure 5), the initialization points at $\omega = 2.5\,\mathrm{rad{\cdot}s^{-1}}$ is also termed S-curve in continuation theory due to its particular shape [4, 34]. In Figure 6, this isola solution curve no longer has this specific shape. The two isolas obtained in Figure 4 are represented and exist up to 0.8 N.

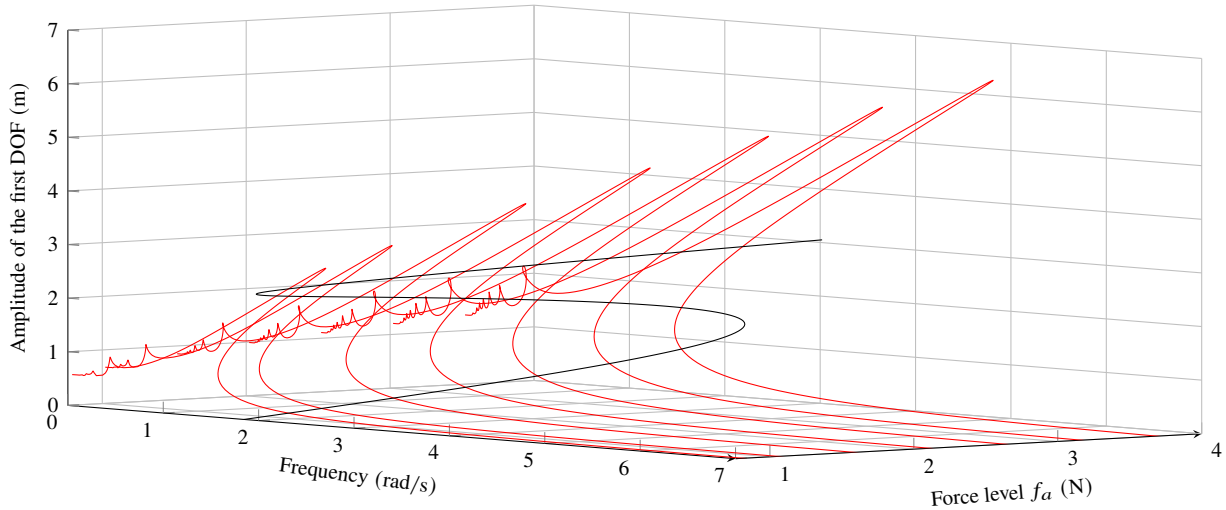

Figure 5. Multiple NFRC for various excitations amplitudes, NFRC (—), primary FAR (—)

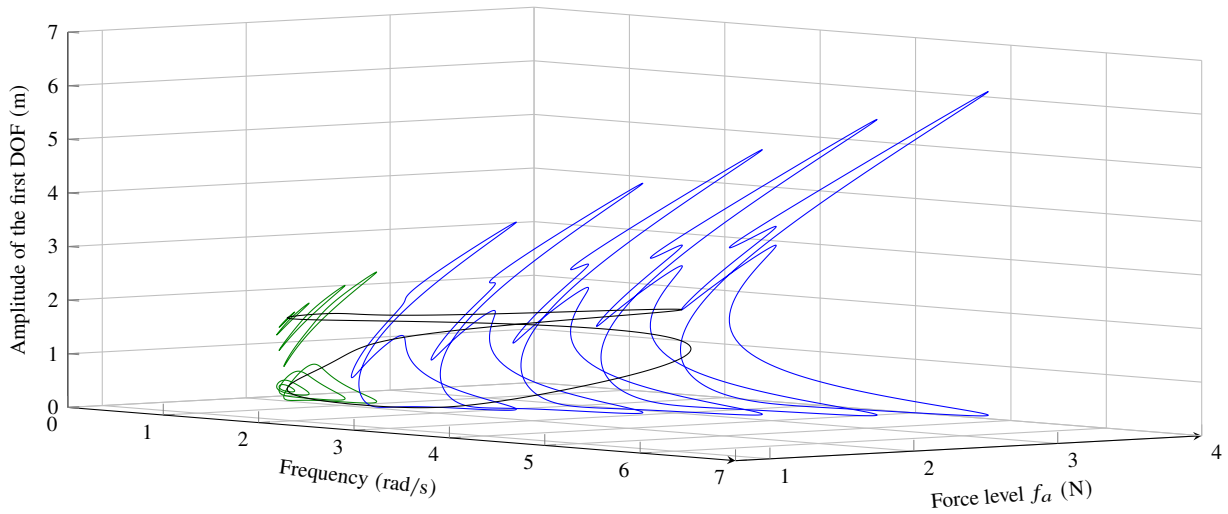

Figure 6. Multiple isolas for various excitations amplitudes, isolas (—) which turn (at high excitation amplitudes) into bifurcated branches (—), bifurcated FAR (—)

As shown in Figures 2b and 6, the isolated curves merge with each other and with the main branch of solution at higher excitation level. Notice that those bifurcation points could have been tracked [24, 25] to follow their evolution and possibly also found the isolas by a different method. The approach proposed in this work is able to compute the isolas without resorting to bifurcation tracking which doubles the size of the problem and requires the computation of the hessian tensor at each iteration of the computation. Moreover, as shown in the next section, it is able to retrieve completely isolated solutions (branch of solution which do no merge with the main response or bifurcated branches for a high forcing amplitude).

4 Robustness of the approach: a plurality of examples

This section aims to present the versatility of the proposed strategy to obtain other kinds of isolas and nonlinearities. First the cyclic Duffing oscillator is investigated to retrieve subharmonic, and ultra-subharmonic isolated solutions. Then a more challenging example is studied: an academic test case with an impact law. Such systems exhibit different resonances curves including period doubling.

4.1 Superharmonic, subharmonic and ultrasubharmonic isolas

So far, the proposed approach was shown to retrieve $1:1$ resonances. However, different kinds of resonances exist, i.e. $k:1$ superharmonic resonances as shown in Figure 4, $1:\nu$ subharmonic, and $k:\nu$ ultra-subharmonic resonances [1]. To retrieve such solutions, the proposed approach can be employed by choosing the appropriate harmonic $a_{\nu,k}$ in Equation Eq. (23).

The mechanical system depicted in Figure 1 is considered with a new damping value $c = 0.01$. The FAR is evaluated for $\omega = 3.5\,\mathrm{rad{\cdot}s^{-1}}$, $k = 1$, and $\nu = 3$. The result of this $1:3$ subharmonic resonance is provided in Figure 7. From the $1:3$ subharmonic resonance arises two bifurcated curves which correspond to $2:3$ ultra-subharmonic resonances.

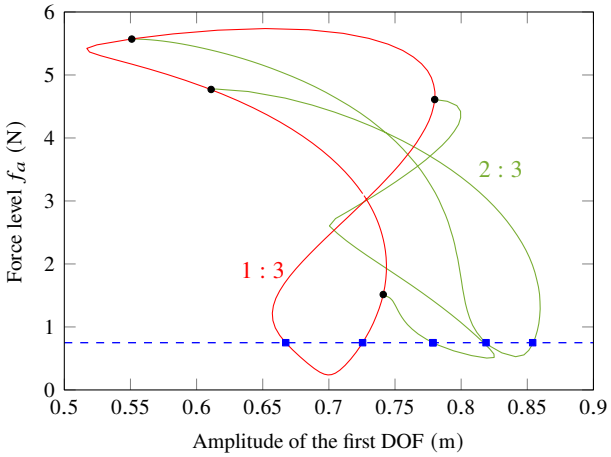

Figure 7. FAR for $\omega = 3.5\,\mathrm{rad{\cdot}s^{-1}}$ with $k = 1$, and $\nu = 3$, primary response curve (—), bifurcated branches (—), bifurcation points (●), $f_a = 0.75\,\mathrm{N}$ (- -), and initialization points for future NFRC (■).

Next, the NFRC of the system is computed with an excitation amplitude of 0.75 N. Beside the primary response, the continuation procedure was employed with the four initialization points of Figure 7 (■). The results are provided in Figure 8. From the four initialization points, both $1:3$ and $2:3$ isolas are obtained. Notice that such results could not have been retrieved through bifurcation tracking [24, 25] because these isolas do not merge with the primary response frequency. These results clearly show the versatility of the proposed approach.

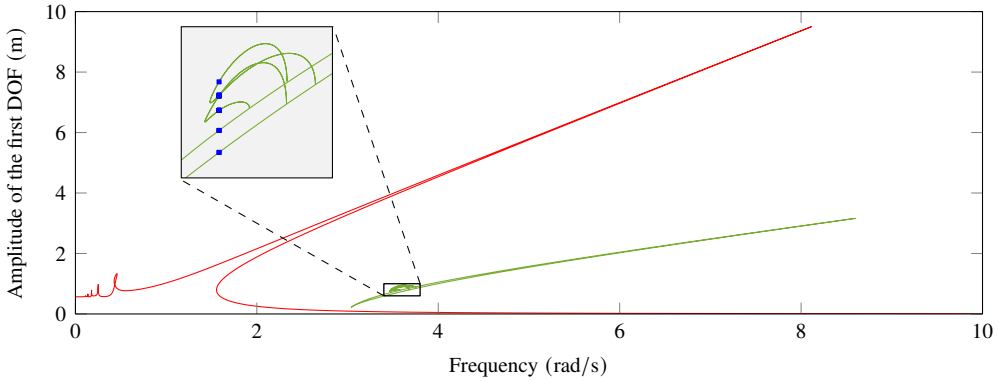

Figure 8. NFRC for an excitation of 0.75 N. primary resonance (—) isolated branches of solutions (—), and initialization points (■). The inset box with gray background corresponds to a close-up of the NFRC on a specific frequency range.

The potential of the proposed strategy to retrieve ultra-subharmonic resonances is highlighted in Figure 9 where different FAR are represented at $7\,\mathrm{rad{\cdot}s^{-1}}$. This figure was obtained through the algorithm presented in Section 3.1 which was run for all (k,ν) in $[\![1,7]\!] \times [\![1,7]\!]$. A loop on the initialization on $a_{k,\nu}$ was run ranging from 0.1 to 10 with an amplitude step of 0.1. A large number of sub and ultra-sub resonances are obtained. For low level of excitation amplitudes (below 10 N), three isolas exist: $1:3$, $4:7$, and $2:3$. Notice also that the $2:3$ ultra-sub harmonic is now detached from the $1:3$ curve. A $3:1$ superharmonic resonance is also observed at high level of forcing amplitudes. This branch of solutions is not closed on itself as the $3:1$ superharmonic resonance is attached to the primary response curve.

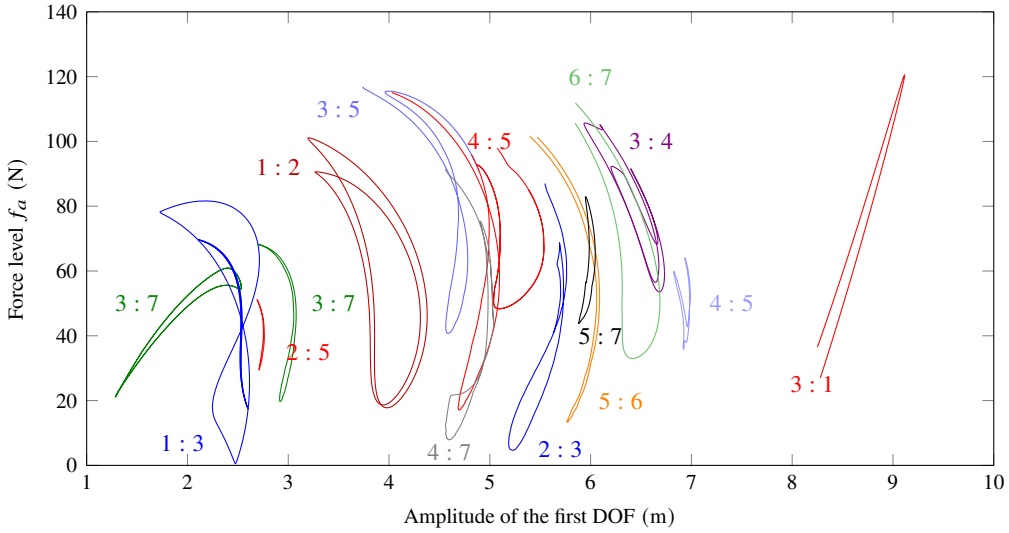

Figure 9. FAR for $\omega = 7\,\mathrm{rad{\cdot}s^{-1}}$ for different sub, ultra-sub and superharmonic resonances.

Figure 9 provides plenty of information on the different solutions of the system. First, the FAR allows to predict the different solutions of the problem for different values of the forcing amplitude for a given excitation frequency. Second, if one is interested in the computation of solutions for a large frequency range, the proposed strategy can be employed for different values of ω. Figure 10 provides an example of NFRC for an excitation amplitude of 3 N. To highlight the potential of the proposed methodology, a few ultra-sub harmonics are computed.

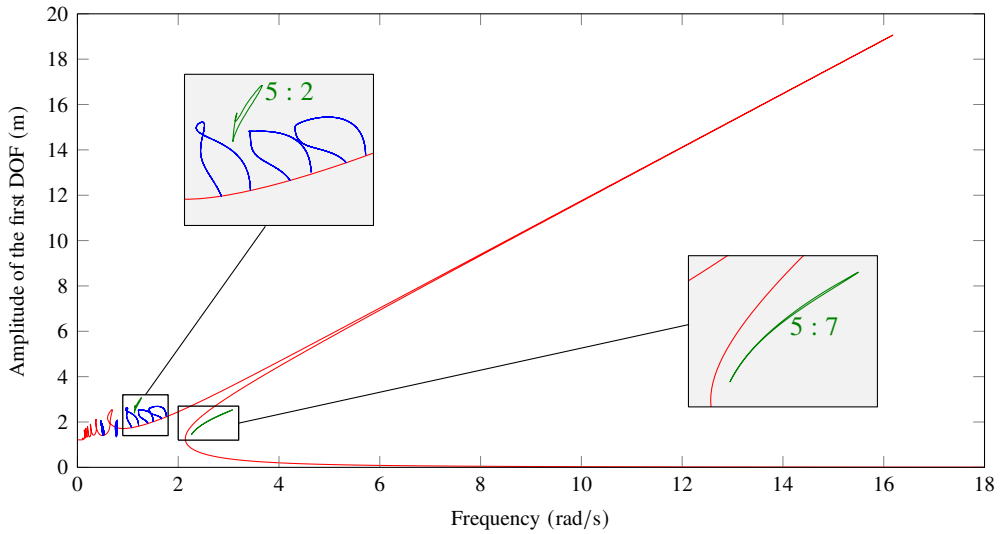

Figure 10. NFRC for an excitation amplitude of 3 N, primary response curve (—) associated bifurcated branches (—), and some ultra-subharmonic resonances (—). The inset boxes with gray background correspond to close-up of the NFRC on specific frequency ranges.

4.2 Impact nonlinearities

To show the versatility of this approach, impact nonlinearities are studied in this section. In this work, a regularized contact law is considered [35, 36],

$$\mathbf{f}_{\mathrm{nl}} = -\kappa \frac{(g_0 - x(t))}{2} + \sqrt{\left(\kappa \frac{(g_0 - x(t))}{2}\right)^2 + \gamma^2} \tag{25}$$

with $\kappa = 1 \cdot 10^4\,\mathrm{N{\cdot}m^{-1}}$, $\gamma = 1 \cdot 10^{-5}\,\mathrm{N}$ and $g_0 = 0.4\,\mathrm{m}$. The parameters respectively stand for the penalization stiffness, the regularization rate, and the initial gap. With this formulation, the first and second derivatives of the nonlinear forces can be derived analytically. The mechanical system under study is depicted in Figure 11. The values of the first and second masses are taken equal to $m_1 = 0.5\,\mathrm{kg}$ and $m_2 = 1\,\mathrm{kg}$ respectively. The first and second stiffness values are equal to $k_1 = 100\,\mathrm{N{\cdot}m^{-1}}$ and $k_2 = 300\,\mathrm{N{\cdot}m^{-1}}$. The damping values are chosen to get a 1% modal damping. In this paper, the first mode located at $\omega = 7.5\,\mathrm{rad{\cdot}s^{-1}}$ is studied. The excitation shape was chosen to excite the first mode

$$\mathbf{f}_{\mathrm{s}} = \mathbf{M}\phi_1, \tag{26}$$

where ϕ_1 is the first mode shape of the system. The HBM is employed with $N_h = 40$ harmonics and the period is discretized through 10^4 instants for the AFT procedure. A similar example was used in [17].

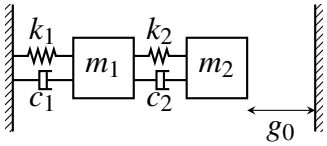

Figure 11. Mechanical system with impact nonlinearities.

As an initial result, Figure 12 shows the FAR for three different values of the excitation frequency: $\omega = 7.5\,\mathrm{rad{\cdot}s^{-1}}$, $\omega = 9\,\mathrm{rad{\cdot}s^{-1}}$, and $\omega = 11\,\mathrm{rad{\cdot}s^{-1}}$. The results of each curve are very different from each other. The curve at $\omega = 7.5\,\mathrm{rad{\cdot}s^{-1}}$ is monotonic, whereas the other two curves present ranges of excitation amplitudes where several solutions exist simultaneously. In addition, within the range $[22\,\mathrm{N}, 30\,\mathrm{N}]$, five different solutions exist for $\omega = 11\,\mathrm{rad{\cdot}s^{-1}}$.

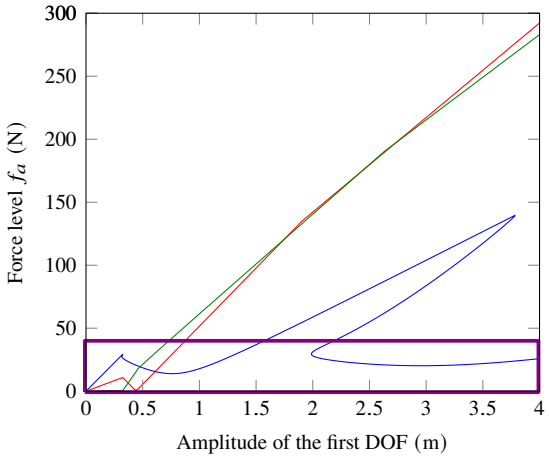

(a) Full simulation.

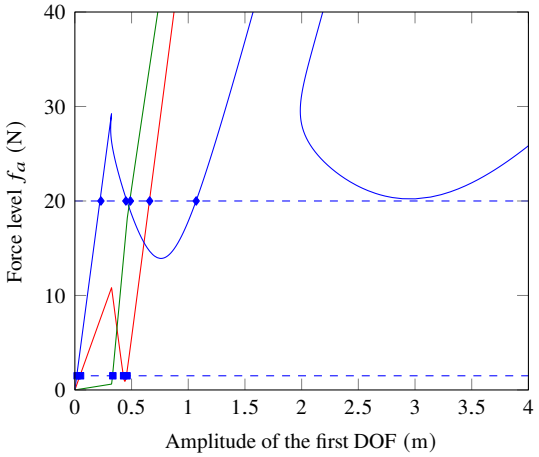

(b) Close-up of the purple rectangle in Figure12a. $f_a = 1.5\,\mathrm{N}$ and $f_a = 20\,\mathrm{N}$ (- -), solutions at $f_a = 1.5\,\mathrm{N}$ (■), and solutions at $f_a = 20\,\mathrm{N}$ (♦).

Figure 12. FAR curve for $\omega = 7.5\,\mathrm{rad{\cdot}s^{-1}}$ (—), $\omega = 9\,\mathrm{rad{\cdot}s^{-1}}$ (—), and $\omega = 11\,\mathrm{rad{\cdot}s^{-1}}$ (—).

These FAR are now used to evaluated NFRCs for two level of excitation amplitude, at 1.5 N, and 20 N. For both excitation amplitudes, the results of Figure 12 provide three initialization points for $\omega = 9\,\mathrm{rad{\cdot}s^{-1}}$ and $\omega = 11\,\mathrm{rad{\cdot}s^{-1}}$. The NFRCs are illustrated in Figure 13. Both of them exhibit isolated branches of solutions. However these are two distinct branches of solutions as the isola in Figure 13a is merged with the primary branch of solution in Figure 13b.

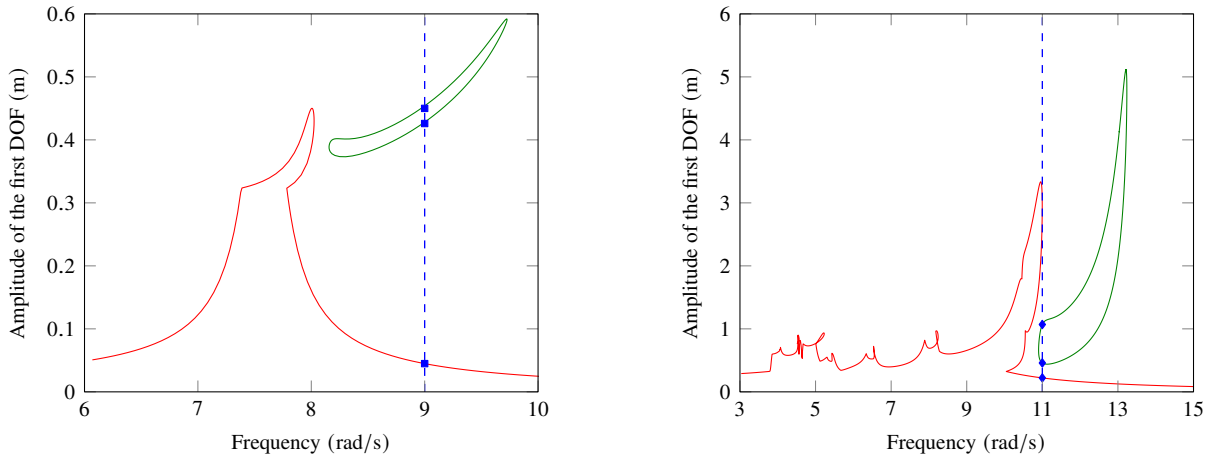

(a) At 1.5 N. **(b)** At 20 N.

Figure 13. NFRC for the mechanical system with impact. Primary response curve (—), isolated branch of solutions (—), and initialization points (♦).

The detection of the isolated branches is very dependent for which values of ω the FAR are computed. For instance, had the FAR been computed at $10.8\,\mathrm{rad{\cdot}s^{-1}}$, the second isola would not have been detected. However, if it had been computed at $10.9\,\mathrm{rad{\cdot}s^{-1}}$, then five initialization points could have been proposed for an excitation amplitude at 20 N: two for the isola and three for the primary response curve. If the excitation frequency is not known, then its value can be swept to evaluate the FAR. Such a procedure is the subject of the following study.

The FAR are now computed from $8\,\mathrm{rad{\cdot}s^{-1}}$ up to $13\,\mathrm{rad{\cdot}s^{-1}}$ with a step of $0.1\,\mathrm{rad{\cdot}s^{-1}}$. Six levels of excitation amplitudes are investigated: 1 N, 5 N, 10 N, 15 N, 20 N, and 25 N. For each of these levels, the NFRCs, based on the initialization points found on the FAR, are computed. To avoid redundancy of the results, the NFRCs are evaluated from initialization points which were not already retrieved from previous simulations. The results are summarized in Figure 14. For better readability, only a few relevant FAR were illustrated.

The results show that the FAR allow to determine three families of isolas which gets merged with the primary response curve as the level of excitation amplitude increases. An isola, which was not previously detected, is now found around $10.5\,\mathrm{rad{\cdot}s^{-1}}$ for an excitation amplitude varying between 10 N and 15 N. Those results are consistent with a previously published work [17] where the isolated branches were computed with Melnikov analysis [15].

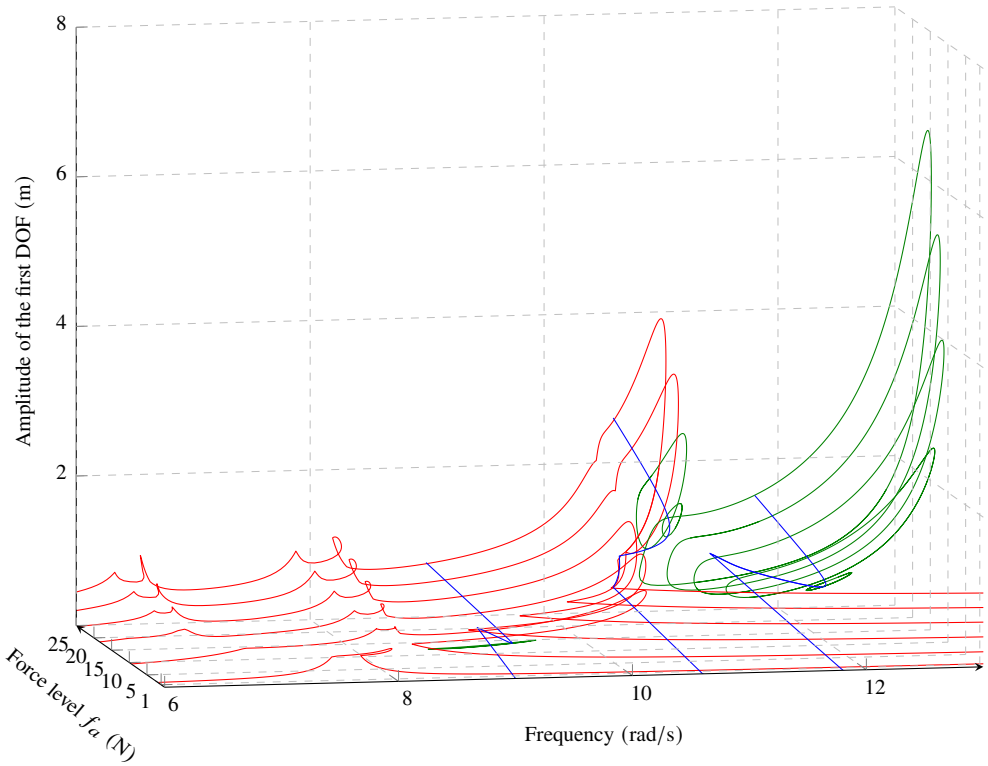

Figure 14. NFRCs and FAR for multiples excitation frequencies and amplitudes. primary resonance (—), isola (—), and FAR (—).

Contact nonlinearities are prone to period doubling bifurcations [26]. This nonlinear phenomena is investigated in what follows. For different values of ω, the FAR are evaluated with $\nu = 2$ and $k = 2$. Figure 15 illustrates some of these results. The primary response curves in red are identical to the ones obtained with $\nu = 1$ and $k = 1$. However, the bifurcated branches (represented in different shades of green) that are obtained correspond to period doubling.

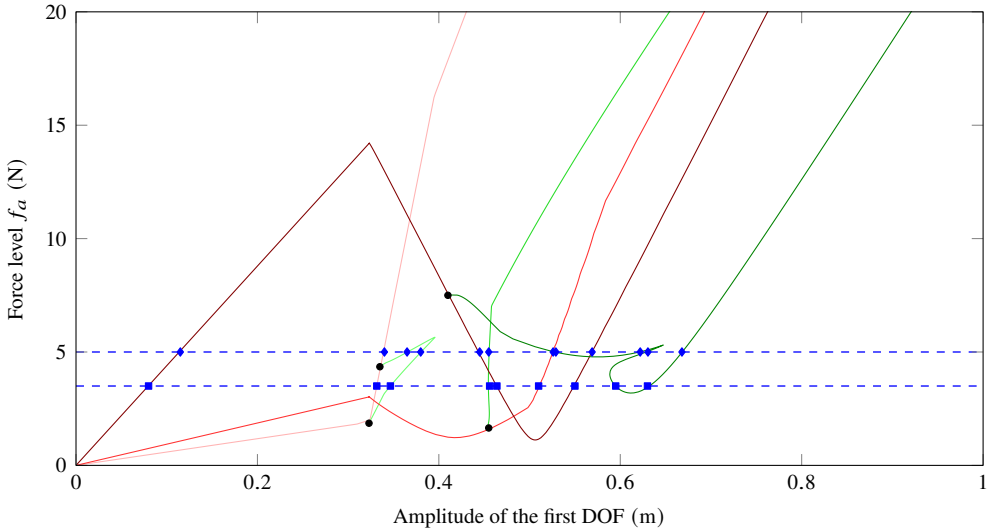

Figure 15. FAR for the contact nonlinearities with $\nu = 2$ and $k = 2$. FAR curves for the main and bifurcated branches for $\omega = 7.3\,\mathrm{rad{\cdot}s^{-1}$ (—)(—), for $\omega = 8\,\mathrm{rad{\cdot}s^{-1}$ (—)(—) and for $\omega = 9.4\,\mathrm{rad{\cdot}s^{-1}$ (—)(—), bifurcation points (●), initialization points for 3.5 N (■) and 5 N (♦).

Next, the NFRC of the system is evaluated for an excitation amplitude equal to 3.5 N and is represented in Figure 16. The initialization points for the NFRC are those of the FAR illustrated in Figure 15 through square markers (■). Two new kinds of solutions are observed: an isolated branch around $9.4\,\mathrm{rad{\cdot}s^{-1}$, and three bifurcated branches. The first two bifurcated branches (at $7.5\,\mathrm{rad{\cdot}s^{-1}$ and $8.3\,\mathrm{rad{\cdot}s^{-1}$) were obtained with the FAR initialization. However, the one located close to $9.3\,\mathrm{rad{\cdot}s^{-1}$ was obtained through the branch switching algorithm from the primary response curve. It could have been retrieved with the FAR but it would have required to sweep the FAR curves with a smaller step of ω.

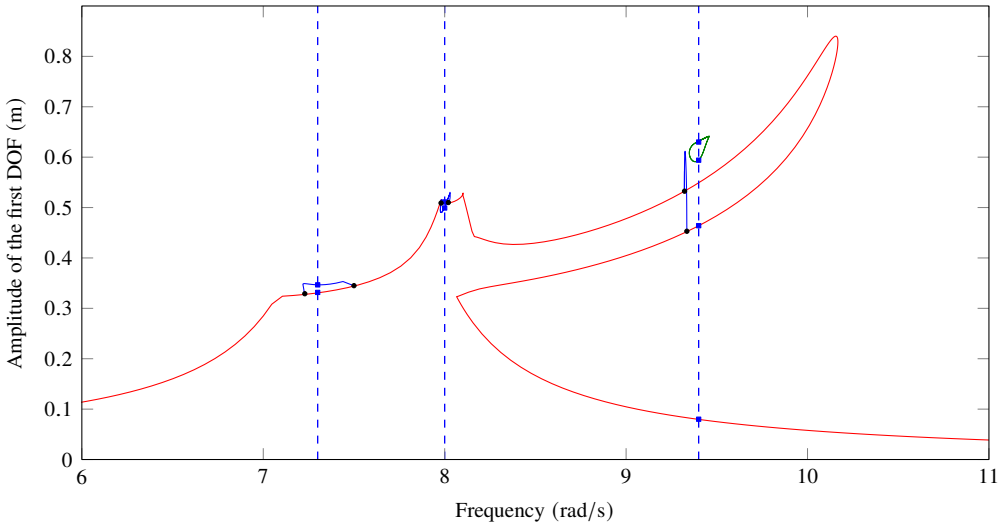

Figure 16. NFRC with a 3.5 N excitation level, primary response curve (—), isola (—), bifurcated branches (—), bifurcation points (●), and initialization points (■).

The excitation amplitude is now increased to 5 N and the NFRC is depicted in Figure 17. The FAR initialization points (diamond markers (♦) in Figure 15) allow to retrieve two isolated branches around $7.5\,\mathrm{rad{\cdot}s^{-1}$ and $10\,\mathrm{rad{\cdot}s^{-1}$.

Three bifurcated branches are also computed.

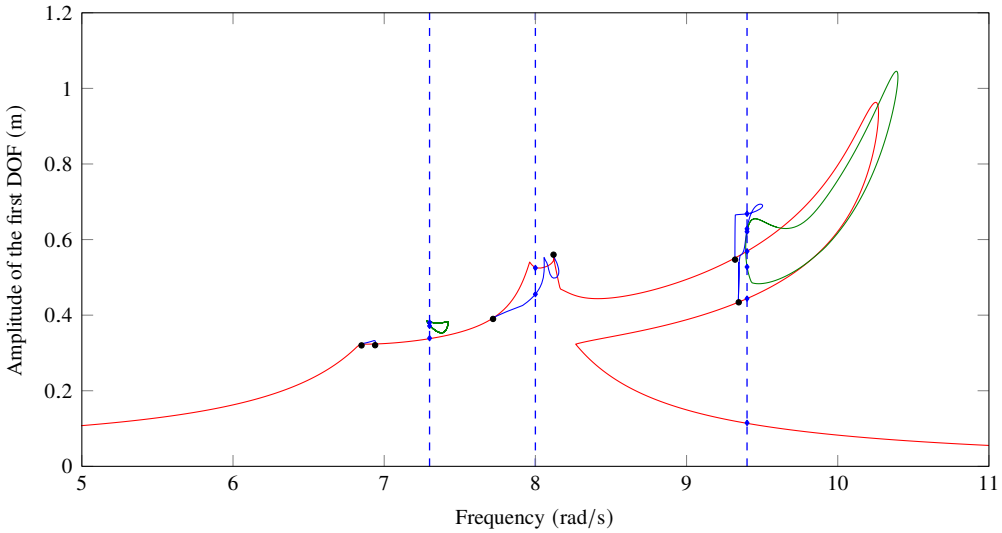

Figure 17. NFRC with a 5 N excitation level, primary response curve (—), isolas (—), bifurcated branches (—), bifurcation points (●), and initialization points (■).

4.3 Short summary of the FAR results

Through the two mechanical systems illustrated in Figures 1 and 11, the proposed strategy was shown to be able to recover multiple types of isolas: primary resonance but also super, sub and ultra-sub harmonic resonances, as well as period doubling bifurcations and isolated branches. The shape of the FAR greatly differ from the type of studied resonances leading to three types of isolas. The first kind is the one which, at high forcing amplitude, merge with the primary resonance through a branching point. For this case, the FAR presents similar behaviour: a bifurcated branch is obtained from the primary curve (see Section 3.2). The second kind is isola which merges and thus becomes the primary resonance at high forcing. For this type of solutions, the FAR presents only a primary curve (see Section 4.2, Figure 14). Finally, the third type of isolas is the one which remains completely detached from other solutions responses. For this situation, the FAR presents identical behaviour: the curve remains also isolated from other curves (see Section 4.1). To obtain such a curve, an initialization of the desired resonance must be given.

The proposed approach computes the FAR at a specific ω value. By sufficiently discretizing the frequency range of interest, all isolas can be detected. However this can become cumbersome if the frequency range is wide.

5 Application to an industrial case

The new methodology was shown to be very interesting to compute complex nonlinear dynamics. The focus of this current section is to show that it can also be applied to large scale systems, and thus to demonstrate the full potential of this approach.

5.1 Presentation of the model

In this section, the proposed approach is applied to ECL5/Catana fan blade [37]. The finite-element model of the blade is illustrated in Figure 18. The latter contains almost 14000 nodes and is clamped at its root. A Craig-Bampton reduction approach [38] is used with 40 internal modes of vibrations and 12 master nodes are kept. Eleven of them are at the tip of the intrados kept for contact treatment purposes, and a node is at the mid-span in order to apply the excitation.

The blade is assumed to be located close to a statoric part (see Figure 19) and hence contact nonlinearities at the blade tip are included in the model. The nodes of the finite element system have three degrees of freedom:

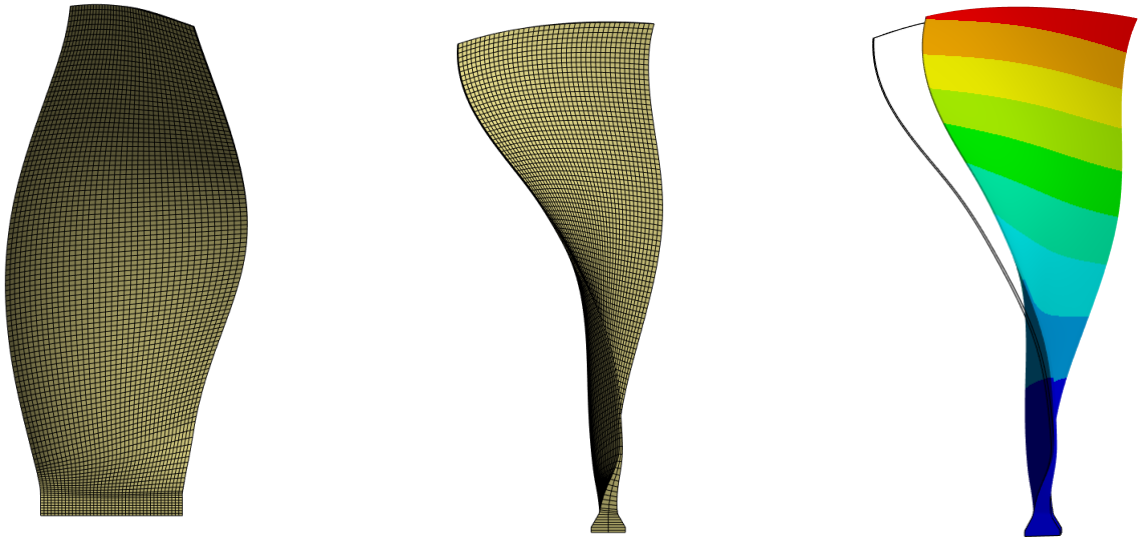

(a) Front view. **(b)** Side view. **(c)** First bending mode.

Figure 18. Catana finite-element model.

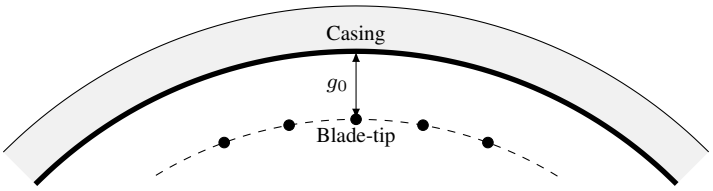

Figure 19. Blade-tip/casing contact.

along the radial (noted N), orthoradial (noted T_1), and axial (noted T_2) directions. The nonlinear force, $\mathbf{f}_{\mathrm{nl,N}}$, in the radial direction is evaluated through Equation Eq. (25). Friction forces are also evaluated for the tangential directions by assuming permanent sliding. For a node i, it leads to

$$\begin{aligned} \mathbf{f}_{\mathrm{nl},\mathrm{T}_1,i} &= \mu\,|\mathbf{f}_{\mathrm{nl,N},i}|\,\frac{v_{\mathrm{T}_1,i}+r_i\omega}{\sqrt{\left(v_{\mathrm{T}_1,i}+r_i\omega\right)^2+\left(v_{\mathrm{T}_2,i}\right)^2}} \\ \mathbf{f}_{\mathrm{nl},\mathrm{T}_1,i} &= \mu\,|\mathbf{f}_{\mathrm{nl,N},i}|\,\frac{v_{\mathrm{T}_2,\mathrm{i}}}{\sqrt{\left(v_{\mathrm{T}_1,i}+r_i\omega\right)^2+\left(v_{\mathrm{T}_2,i}\right)^2}}, \end{aligned} \tag{27}$$

where μ is the friction coefficient, and $v_{\mathrm{T_j,i}}$ is the velocity of node i in the direction j. For the orthoradial direction, the rotation speed of the system is included through the term $r_i\omega$, where r_i is the radius of node i. The parameters of the nonlinearities are provided in Table 2.

Parameters	μ	γ (N)	g_0 (m)	κ $\left(\mathrm{N{\cdot}m^{-1}}\right)$
Values	0.15	1	$4\cdot10^{-4}$	$1\cdot10^{7}$

Table 2. Contact nonlinearity parameters.

The first bending mode whose resonant frequency is around $1878\,\mathrm{rad{\cdot}s^{-1}}$ is studied in this article.

5.2 Numerical results

The HBM is employed with $N_h = 15$ harmonics and the time period is discretized with 2000 instants. To ensure fast computation, the linear degrees of freedom are substituted through a condensation strategy [39]. The FAR are computed with $\nu = 1$ and $k = 1$, from $1830\,\mathrm{rad{\cdot}s^{-1}}$ to $1890\,\mathrm{rad{\cdot}s^{-1}}$ with a step of $\mathrm{d}\omega = 1$. The results are displayed in Figure 20 and present the interesting features to have a non-monotonous resonant frequency : it increases (hardening), before decreasing (softening). For very low excitation amplitude, several solutions are obtained around $1890\,\mathrm{rad{\cdot}s^{-1}}$ (blue squares (■)). Moreover, with the softening behaviour, at very low excitation frequencies, very high amplitudes solutions can be retrieved (represented by the blue circles (●) around $1840\,\mathrm{rad{\cdot}s^{-1}}$ and 5 N). Without evaluating the NFRCs, it is difficult to state if such points correspond to isolas or not.

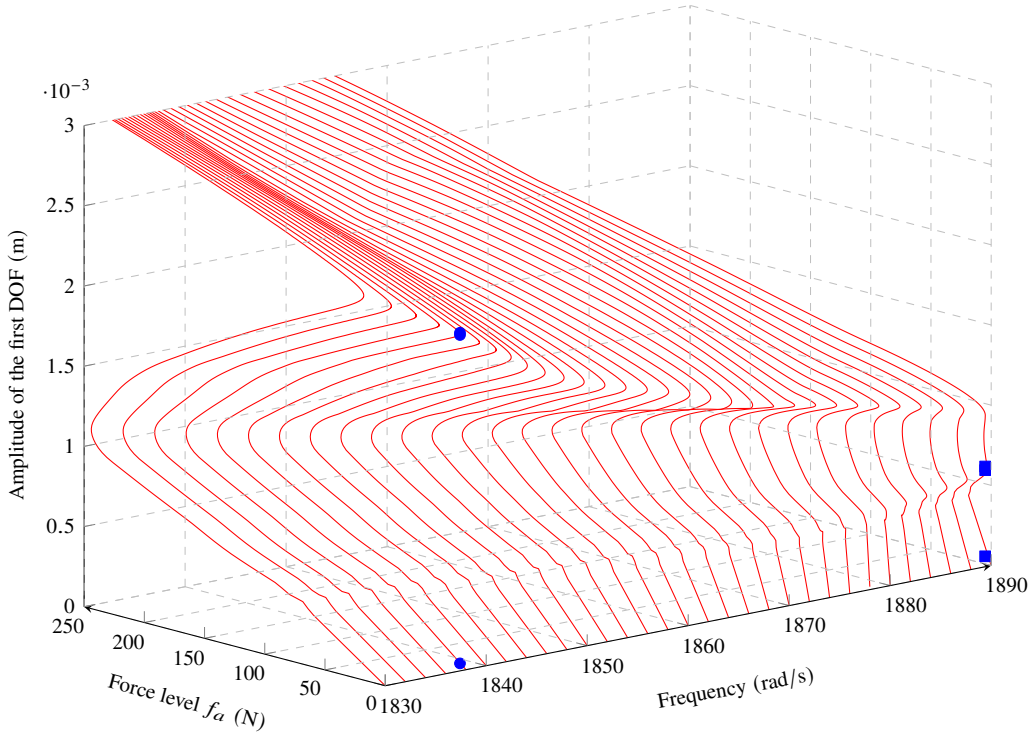

Figure 20. FAR for a large frequency range with $\nu = 1$, and $k = 1$. FAR (—), initialization points for an excitation level of 3.2 N (■) and 5 N (●).

First, the system is excited with an amplitude of 3.2 N. The three points, illustrated through blue squares (■) in Figure 20, are used as initialization points. The results are depicted in Figure 21. An hardening behaviour is observed in the primary response curve (similar to the academic test case studied in Section 4.2) as well as an isolated branch of solution.

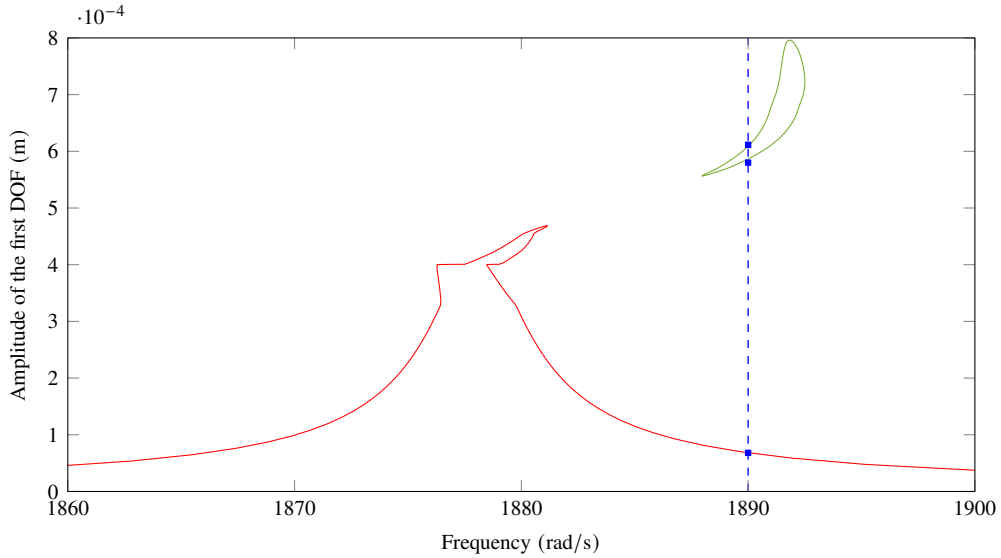

Figure 21. NFRC for a 3.2 N excitation amplitude. primary response curve (—), isola (—), and initialization points (■).

Period doubling bifurcations are also obtained and are retrieved with the FAR computation with $\nu = 2$ and $k = 2$. The results are presented in Figure 22 at 1888 rad·s^{-1}. For a range of excitation amplitudes within [6 N, 12 N], five different solutions exist on the primary response curve. The period doubling bifurcated branch exists between [4 N, 15 N].

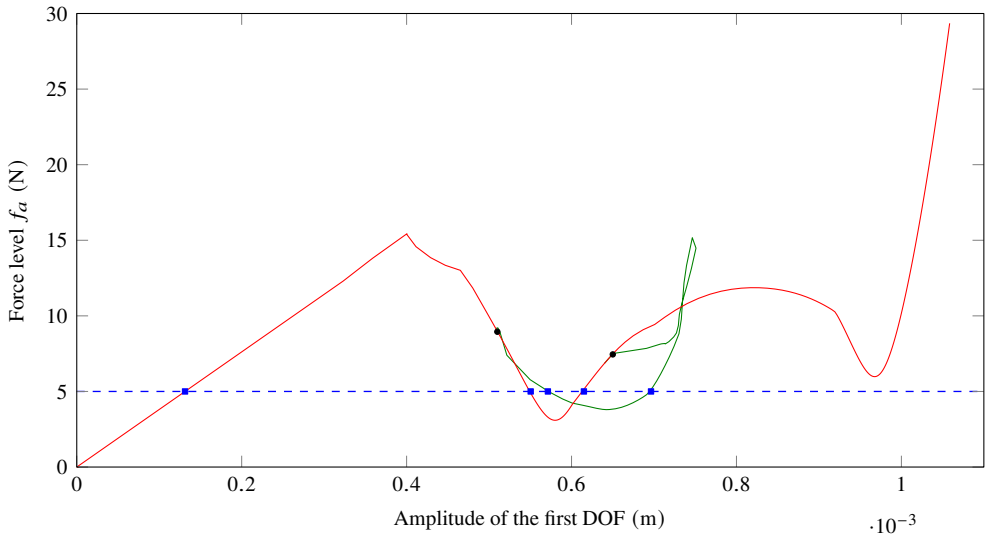

Figure 22. FAR for $\omega = 1888\,\text{rad}\cdot\text{s}^{-1}$ for $\nu = 2$ and $k = 2$, primary response curve (—), period doubling bifurcated branch (—), bifurcations points (●), and initialization points (■).

The NFRC of the system is evaluated for an excitation of 5 N. The initialization points of Figures 20 and 22 are used. The results are presented in Figure 23. The primary response has a hardening behaviour followed by a softening one which explains the three then five possible solutions observed in the FAR curves (see Figure 22). The FAR allows obtaining period doubling bifurcated branches which exhibit a hardening behaviour. Finally, a very high amplitude isolated branch is retrieved at low frequencies (around 1840 rad·s^{-1}). Based on Figure 20, this branch is

expected to merge with the primary response at high level of forcing.

The main difference between the industrial case (see Figure 18) and the academic case (see Figure 11) is the softening behaviour. A possible explanation would be the influence of the friction nonlinearities which are included for the industrial test case. A definitive statement would require further investigations beyond the scope of this paper.

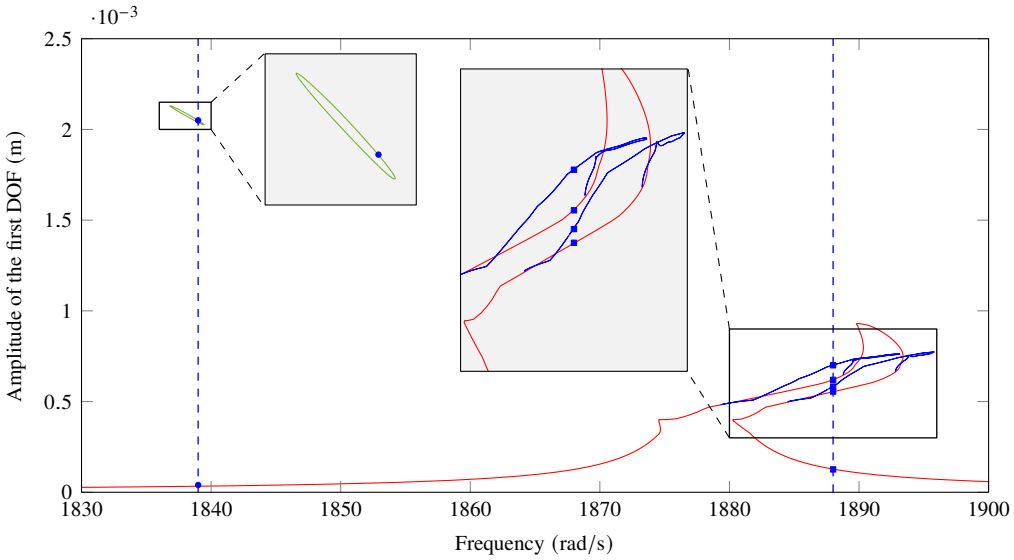

Figure 23. NFRC at 5 N, primary response curve (—), isola (—), and period doubling branches (—), initialization points (■)(●) obtained at 1839 rad·s^{-1} (Figure 20) and 1888 rad·s^{-1} (Figure 22). The inset boxes with gray background correspond to close-up of the NFRC on specific frequency ranges.

6 Conclusion

This paper presents a new methodology to find isolated branches of nonlinear mechanical systems. First, the strategy evaluates FAR curves by imposing the excitation frequency and by initializing on a specific harmonic. A branch switching algorithm is also employed to retrieve bifurcated solutions from the primary response curve. Force amplitude responses offer the possibility to evaluate all possible solutions for any excitation level at a fixed excitation frequency. To evaluate traditional NFRC, one selects the forcing amplitude, retrieves the possible solutions from the FAR, and initializes the continuation procedure with these solutions.

This strategy has been successfully employed for different kinds of nonlinearities: cubic, impact, and blade-tip casing contacts. The methodology has been able to retrieve isolated solutions of many kinds: 1 : 1 isolas, superharmonic, subharmonic, ultrasub-harmonic resonances, and period doubling solutions. The FAR curves have different shapes and behaviour depending on the nonlinearity. Three kinds of isola were observed in the NFRC: those who merge with the primary resonance through branching points, those who merge and become the primary resonance, and finally those who remain isolated. For the two former cases, the merge occur at high forcing level.

The proposed method has been successfully applied to complex and large scale systems (cyclic structures, industrial blades) with a large number of harmonics. This approach is thus very versatile and present high potential to compute isolas. It is expected to enhance the understanding of nonlinear dynamics, but also to be used to find new solutions for any mechanical systems.

Future works would consist in evaluating the influence of the choice of the DOF whose amplitude is imposed for the FAR evaluation. Applying this method to retrieve localized vibration for mistuned cyclic systems would also be an interesting avenue of research. Another prospect would be to use such strategy to obtain isolas experimentally.

Acknowledgement

The authors are thankful for the financial support of the ANR (project ANR-22-CPJ2-0061-01) and the HE-ART project (Grant agreement ID: 101102013).

References

[1] A. H. Nayfeh and D. T. Mook. Nonlinear Oscillations. 2008.

[2] H. Abramson. "Response curves for a system with softening restoring force" (1955).

[3] T. Detroux, J.-P. Noël, L. N. Virgin, and G. Kerschen. "Experimental study of isolas in nonlinear systems featuring modal interactions". PLOS ONE Vol. 13, No. 3 (2018), e0194452. DOI: 10.1371/journal.pone.0194452.

[4] L. Renson, A. D. Shaw, D. A. W. Barton, and S. A. Neild. "Application of control-based continuation to a nonlinear structure with harmonically coupled modes". Mechanical Systems and Signal Processing Vol. 120 (2019), pp. 449–464. DOI: 10.1016/j.ymssp.2018.10.008.

[5] L. Woiwode and M. Krack. "Experimentally uncovering isolas via backbone tracking." Journal of Structural Dynamics (2024). DOI: 10.25518/2684-6500.180.

[6] T. Zhou and G. Kerschen. *Identification of Secondary Resonances of Nonlinear Systems using Phase-Locked Loop Testing*. 2024.

[7] J. Perret-Liaudet and E. Rigaud. "Response of an impacting Hertzian contact to an order-2 subharmonic excitation : Theory and experiments". Journal of Sound and Vibration Vol. 296, No. 1 (2006), pp. 319–333. DOI: 10.1016/j.jsv.2006.03.004.

[8] F. Mangussi and D. H. Zanette. "Internal Resonance in a Vibrating Beam: A Zoo of Nonlinear Resonance Peaks". PLOS ONE Vol. 11, No. 9 (2016), e0162365. DOI: 10.1371/journal.pone.0162365.

[9] G. Habib, G. I. Cirillo, and G. Kerschen. "Isolated resonances and nonlinear damping". Nonlinear Dynamics Vol. 93, No. 3 (2018), pp. 979–994. DOI: 10.1007/s11071-018-4240-z.

[10] S. Ponsioen, T. Pedergnana, and G. Haller. "Analytic prediction of isolated forced response curves from spectral submanifolds". Nonlinear Dynamics Vol. 98, No. 4 (2019), pp. 2755–2773. DOI: 10.1007/s11071-019-05023-4.

[11] M. Krack and J. Gross. "Theory of harmonic balance". *Harmonic Balance for Nonlinear Vibration Problems*. Mathematical Engineering. Cham, 2019, pp. 11–46. DOI: 10.1007/978-3-030-14023-6_2.

[12] A. Grolet and F. Thouverez. "Computing multiple periodic solutions of nonlinear vibration problems using the harmonic balance method and Groebner bases". Mechanical Systems and Signal Processing Vol. 52-53 (2015), pp. 529–547. DOI: 10.1016/j.ymssp.2014.07.015.

[13] T. Heinze, L. Panning-von Scheidt, and J. Wallaschek. "Global detection of detached periodic solution branches of friction-damped mechanical systems". Nonlinear Dynamics Vol. 99, No. 3 (2020), pp. 1841–1870. DOI: 10.1007/s11071-019-05425-4.

[14] R. J. Kuether, L. Renson, T. Detroux, C. Grappasonni, G. Kerschen, and M. S. Allen. "Nonlinear normal modes, modal interactions and isolated resonance curves". Journal of Sound and Vibration Vol. 351 (2015), pp. 299–310. DOI: 10.1016/j.jsv.2015.04.035.

[15] M. Cenedese and G. Haller. "How do conservative backbone curves perturb into forced responses? A Melnikov function analysis". Proceedings of the Royal Society A: Mathematical, Physical and Engineering Sciences Vol. 476, No. 2234 (2020), p. 20190494. DOI: 10.1098/rspa.2019.0494.

[16] S. Benacchio, C. Giraud-Audine, and O. Thomas. "Effect of dry friction on a parametric nonlinear oscillator". Nonlinear Dyn. Vol. 108, No. 2 (2022), pp. 1005–1026. DOI: 10.1007/s11071-022-07233-9.

[17] T. Vadcard, F. Thouverez, and A. Batailly. "On the detection of nonlinear normal mode-related isolated branches of periodic solutions for high-dimensional nonlinear mechanical systems with frictionless contact interfaces". Computer Methods in Applied Mechanics and Engineering Vol. 419 (2024), p. 116641. DOI: 10.1016/j.cma.2023.116641.

[18] T. Vadcard, F. Thouverez, and A. Batailly. "Computation of isolated periodic solutions for forced response blade-tip/casing contact problems". J. Eng. Gas Turbines Power (2023), pp. 1–23. DOI: 10.1115/1.4063704.

[19] M. Peeters, R. Viguié, G. Sérandour, G. Kerschen, and J. C. Golinval. "Nonlinear normal modes, Part II: Toward a practical computation using numerical continuation techniques". Mechanical Systems and Signal Processing. Special Issue: Non-linear Structural Dynamics Vol. 23, No. 1 (2009), pp. 195–216. DOI: 10.1016/j.ymssp.2008.04.003.

[20] R. Seydel. Practical Bifurcation and Stability Analysis. 3rd ed. Interdisciplinary Applied Mathematics. New York, 2010.

[21] E. P. Petrov. "Analysis of Bifurcations in Multiharmonic Analysis of Nonlinear Forced Vibrations of Gas Turbine Engine Structures With Friction and Gaps". Journal of Engineering for Gas Turbines and Power Vol. 138, No. 10 (2016). DOI: 10.1115/1.4032906.

[22] E. P. Petrov. "A Method for Parametric Analysis of Stability Boundaries for Nonlinear Periodic Vibrations of Structures With Contact Interfaces". Journal of Engineering for Gas Turbines and Power Vol. 141, No. 031023 (2018). DOI: 10.1115/1.4040850.

[23] E. Sarrouy, A. Grolet, and F. Thouverez. "Global and bifurcation analysis of a structure with cyclic symmetry". International Journal of Non-Linear Mechanics Vol. 46, No. 5 (2011), pp. 727–737. DOI: 10.1016/j.ijnonlinmec.2011.02.005.

[24] T. Detroux, L. Renson, L. Masset, and G. Kerschen. "The harmonic balance method for bifurcation analysis of large-scale nonlinear mechanical systems". Computer Methods in Applied Mechanics and Engineering Vol. 296 (2015), pp. 18–38. DOI: 10.1016/j.cma.2015.07.017.

[25] L. Xie, S. Baguet, B. Prabel, and R. Dufour. "Bifurcation tracking by Harmonic Balance Method for performance tuning of nonlinear dynamical systems". Mechanical Systems and Signal Processing Vol. 88 (2017), pp. 445–461. DOI: 10.1016/j.ymssp.2016.09.037.

[26] R. Alcorta, S. Baguet, B. Prabel, P. Piteau, and G. Jacquet-Richardet. "Period doubling bifurcation analysis and isolated sub-harmonic resonances in an oscillator with asymmetric clearances". Nonlinear Dynamics Vol. 98, No. 4 (2019), pp. 2939–2960. DOI: 10.1007/s11071-019-05245-6.

[27] C. Grenat, S. Baguet, C. H. Lamarque, and R. Dufour. "A multi-parametric recursive continuation method for nonlinear dynamical systems". Mechanical Systems and Signal Processing Vol. 127 (2019), pp. 276–289. DOI: 10.1016/j.ymssp.2019.03.011.

[28] G. Raze, M. Volvert, and G. Kerschen. "Tracking amplitude extrema of nonlinear frequency responses using the harmonic balance method". International Journal for Numerical Methods in Engineering Vol. 125, No. 2 (2024), e7376. DOI: https://doi.org/10.1002/nme.7376.

[29] A. Mélot, E. Denimal Goy, and L. Renson. "Control of isolated response curves through optimization of codimension-1 singularities". Computers & Structures Vol. 299 (2024), p. 107394. DOI: 10.1016/j.compstruc.2024.107394.

[30] T. M. Cameron and J. H. Griffin. "An alternating frequency/time domain method for calculating the steady-state response of nonlinear dynamic systems". Journal of Applied Mechanics Vol. 56, No. 1 (1989), pp. 149–154. DOI: 10.1115/1.3176036.

[31] E. P. Petrov. "Stability Analysis of Multiharmonic Nonlinear Vibrations for Large Models of Gas Turbine Engine Structures With Friction and Gaps". Journal of Engineering for Gas Turbines and Power Vol. 139, No. 022508 (2016). DOI: 10.1115/1.4034353.

[32] Y. Colaïtis and A. Batailly. "Stability Analysis of an Industrial Blade Accounting for a Blade-Tip/Casing Nonlinear Interface". Journal of Engineering for Gas Turbines and Power Vol. 145, No. 041003 (2022). DOI: 10.1115/1.4055492.

[33] Y. Kuznetsov. Elements of Applied Bifurcation Theory. 3rd ed. Applied Mathematical Sciences. Springer-Verlag. New York, 2004. DOI: 10.1007/978-1-4757-3978-7.

[34] G. Abeloos, L. Renson, C. Collette, and G. Kerschen. "Stepped and swept control-based continuation using adaptive filtering". Nonlinear Dynamics Vol. 104, No. 4 (2021), pp. 3793–3808. DOI: 10.1007/s11071-021-06506-z.

[35] L. Woiwode, N. N. Balaji, J. Kappauf, F. Tubita, L. Guillot, C. Vergez, B. Cochelin, A. Grolet, and M. Krack. "Comparison of two algorithms for Harmonic Balance and path continuation". Mechanical Systems and Signal Processing Vol. 136 (2020), p. 106503. DOI: 10.1016/j.ymssp.2019.106503.

[36] Y. Colaïtis and A. Batailly. "The harmonic balance method with arc-length continuation in blade-tip/casing contact problems". Journal of Sound and Vibration Vol. 502 (2021), p. 116070. DOI: 10.1016/j.jsv.2021.116070.

[37] V. Pagès, P. Duquesne, S. Aubert, L. Blanc, P. Ferrand, X. Ottavy, and C. Brandstetter. "UHBR Open-Test-Case Fan ECL5/CATANA". International Journal of Turbomachinery, Propulsion and Power Vol. 7, No. 2 (2022). Number: 2 Publisher: Multidisciplinary Digital Publishing Institute, p. 17. DOI: 10.3390/ijtpp7020017.

[38] R. Craig and M. Bampton. "Coupling of substructures for dynamic analyses." AIAA Journal Vol. 6, No. 7 (1968), pp. 1313–1319. DOI: 10.2514/3.4741.

[39] O. Poudou and C. Pierre. "Hybrid frequency-time domain methods for the analysis of complex structural systems with dry friction damping". *44th AIAA/ASME/ASCE/AHS/ASC Structures, Structural Dynamics, and Materials Conference*. DOI: 10.2514/6.2003-1411.